The virtual seismometer method: Its theory, history, and promise

Jens-Erik Lund Snee

***Abstract*—The virtual seismometer method (VSM), also called inter-source seismic interferometry, is a technique for finding the Green function between nearby earthquakes by estimating the response that would be detected at one earthquake location if it were a seismometer observing the others. This promising new type of seismic interferometry has found diverse applications in the past several years, although applications are surprisingly few considering the power of the technique. In this paper, I summarize the history of seismic interferometry and also the specific case of VSM. I provide the theoretical basis for both of these techniques, as well as several recent applications, most notably for continued methods development in the field of seismic interferometry. This report is intended to highlight ways that VSM can advance active research in the geosciences. Most notably, VSM has potential to dramatically improve studies of the path and source properties in areas experiencing microseismicity (including for geothermal and unconventional oil and gas production applications), and also in remote areas that have historically received less attention and instrumentation, such as under oceans.**

I. Introduction: Virtual seismometers

THE virtual seismometer method (VSM) is a technique that treats an energy source (an earthquake) as a receiver. Put differently, it is a means to find the signal that would be detected at one earthquake location if it were a seismometer recording the signal of another earthquake. This technique is one form of seismic interferometry (Schuster, 2001), in which, historically, the Green function (defined below) between seismometers has been found by crosscorrelating noise or earthquake *coda waves* (the late parts of seismic waves) between pairs of sensors (Figure 1). Using the principles of traditional seismic interferometry, Curtis et al. (2009) proposed a technique for estimating the Green function between two nearby *earthquakes*, treating one of these events as a "virtual seismometer." This technique, which is something of the converse of conventional seismic interferometry, involves crosscorrelating the coda waves between pairs of earthquakes recorded at a single station, repeating this process for multiple stations, and then stacking the results to find the Green function between each earthquake pair. This procedure can be repeated for any number of nearby earthquakes to estimate the path parameters between them, hence potentially populating the subsurface in an area with this information, even if seismometers are sparse.

In this document, I present the history and theoretical background of this promising new technique, and then I discuss its potential uses to advance topics of active research. Because VSM is an outgrowth of seismic interferometry, which is itself a major topic of interest in the geosciences, I first provide some general technical background before detailing the theoretical underpinnings and historical development of seismic interferometry, leading up to the formal introduction of VSM by Curtis et al. (2009). I then summarize the theoretical basis for the technique given by these authors, followed by a discussion of ways that it has recently been applied to academic and industry research. I conclude by offering my views regarding the most promising potential applications of VSM for answering geoscience questions.

II. Background

A. The Green function

For background, the Green function is defined as the response —/\/\— at a receiver due to a unit point displacement ⊥ at a source. Put more simply, the Green function is the impulse response of a point source detected at a receiver location. As described in the course notes and, for example, by Kwiatek et al. (2016), the Green function tensor, $\mathbf{G}$, relates particle displacement, $\mathbf{u}(\mathbf{x}, t)$,

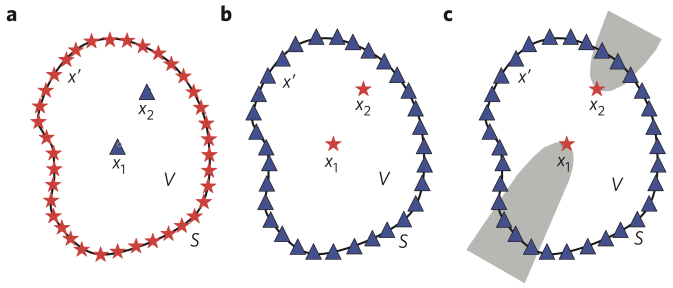

Fig. 1: Schematic diagrams from Curtis et al. (2009) depicting source–receiver geometries for seismic interferometry. Red stars are sources or virtual sources; blue triangles are receivers or virtual receivers. (a). Classic seismic interferometry in which the Green function is calculated between two receivers using the crosscorrelated coda from multiple earthquakes (see Campillo and Paul, 2003). (b). The newer method of constructing "virtual seismometers" (VSM) to estimate the Green functions between energy sources, introduced by Curtis et al. (2009). (c). Unfortunately, virtual seismometers can only be constructed at sources located approximately along the line connecting the virtual receivers x_1 and x_2, represented by the grey zones.

to the radiated energy in the form of the moment tensor, $\mathbf{M}$, through

$$\mathbf{u}(\mathbf{x},t) = \mathbf{M} * \mathbf{G}, \tag{1}$$

where $*$ denotes convolution in the time domain (Madariaga, 2007). Before obtaining the expression for $\mathbf{G}$, we can solve the elastodynamic wave equation to find the full (rather complicated) expression for the seismic radiation from a point source:

$$\begin{aligned}\mathbf{u}(R,t) = {} & \frac{1}{4\pi\rho}\left[\mathbf{f}\cdot\nabla\nabla\left(\frac{1}{R}\right)\right]\int_{R/\alpha}^{\min(t,R/\beta)} \tau s(t-\tau)\mathrm{d}\tau \\ & + \frac{1}{4\pi\rho a^2}\frac{1}{R}\left(\mathbf{f}\cdot\nabla R\right)\nabla R s\left(t-R/\alpha\right) \\ & + \frac{1}{4\pi\rho\beta^2}\frac{1}{R}\left[\mathbf{f}-\left(\mathbf{f}\cdot\nabla R\right)\nabla R\right] s\left(t-R/\beta\right),\end{aligned} \tag{2}$$

where $R = \|\mathbf{x}-\mathbf{x}_0\|$ is the distance from the earthquake source, $\mathbf{x}_0$, to the receiver, $\mathbf{x}$, t is time, $\mathbf{f}(\mathbf{x},t) = \mathbf{f}s(t)\delta\left(\mathbf{x}-\mathbf{x}_0\right)$ is force density, $s(t)$ is the source time function, $\alpha = \sqrt{(\lambda+2\mu)/\rho}$ is the P-wave velocity, $\beta = \sqrt{\mu/\rho}$ is the S-wave velocity, λ is the Lamé constant, μ is the shear modulus, and ρ is density (Madariaga, 2007). The latter two terms describe the response in the far-field, and the first term describes the response in the near-field. An infinite, isotropic, linear elastic medium is assumed at present.

Now that we have an expression for seismic radiation from a point source, we follow the procedure described by Madariaga (2007) to find the Green tensor, $\mathbf{G}$, for elastic waves under these conditions using the simple relationship

$$\mathbf{u}(\mathbf{x},t) = \mathbf{G}\left(\mathbf{x},t|\mathbf{x}_0,0\right)\cdot\mathbf{f} * s(t). \tag{3}$$

In index notation,

$$\begin{aligned}G_{ij}\left(\mathbf{x},t|\mathbf{x}_0,0\right) = {} & \frac{1}{4\pi\rho}\left(\frac{1}{R}\right)_{,ij} \\ & \times t\left[H\left(t-R/\alpha\right)-H\left(t-R/\beta\right)\right] \\ & + \frac{1}{4\pi\rho\alpha^2}\frac{1}{R}\left(R_{,i}R_{,j}\right)\delta\left(t-R/\alpha\right) \\ & + \frac{1}{4\pi\rho\beta^2}\frac{1}{R}\left(\delta_{ij}-R_{,i}R_{,j}\right)\delta\left(t-R/\beta\right),\end{aligned} \tag{4}$$

where δ_{ij} is the Kronecker delta and $\delta(t)$ is the Dirac delta.

B. The moment tensor

The moment tensor, $\mathbf{M}$, describes the geometry and magnitudes of forces applied at the source. $\mathbf{M}$ is symmetrical and of the form

$$\mathbf{M} = \begin{bmatrix} M_{xx} & M_{xy} & M_{xz} \\ M_{yx} & M_{yy} & M_{yz} \\ M_{zx} & M_{zx} & M_{zz} \end{bmatrix}, \tag{5}$$

where each component refers to a single force couple, with each a pair of equal and opposite forces acting in the i direction and separated in the j direction (see Madariaga, 2007, and Curtis et al., 2009). Inserting the definitions for $\mathbf{G}$ and $\mathbf{M}$ into Equation 1, we have

$$u_k(\mathbf{x},t) = \sum_{ij} G_{ki,k}\left(\mathbf{x},t|x_0,t\right) * M_{ij}(t). \tag{6}$$

III. Historical development and basic procedure

The rapidly advancing field of seismic interferometry (Schuster, 2001) provides the basis for VSM described here. Defined broadly, *interferometry* is the use of wave interference to obtain useful signal information. *Seismic interferometry* more specifically takes advantage of constructive or destructive interference of seismic waves that are multiply scattered by the heterogeneous

subsurface during their propagation (Snieder, 2004). Seismic interferometry typically involves the use of crosscorrelation (or, in some cases, convolution) of seismic responses observed at different receivers to determine the Green function and other characteristics between receivers (Wapenaar et al., 2010). Most commonly, this technique is applied to data contained within the seismic coda or to the ambient seismic field (ASF or "ambient noise"). The coda wave contains complicated energy produced by energy scattering as waves pass through an inhomogeneous medium (Aki, 1969; Aki and Chouet, 1975; Sato, 1977; Aki, 1980). The multiply scattered wave energy contained in the coda cannot be understood using classical seismological theory, which describes the *ballistic* (direct and nonscattered, as opposed to *diffuse* seismic energy) portion of seismic waveforms, but the use of crosscorrelation and similar techniques on pairs of seismic traces has enabled seismologists to extract the path and source parameters between points out of this complicated signal.

A. Early advancements

The first application of interferometry to seismology is sometimes traced to a paper by Claerbout (1968) that proposed that, for a seismogram observed on the surface of the Earth that resulted from an impulsive source, *autocorrelating*—crosscorrelating the signal with itself—will produce the same result regardless of whether the pulse was generated somewhere else on the surface of the Earth or somewhere beneath the receiver, in the infinite half-space below a layered medium. Rickett and Claerbout (1999) proved this suggestion for the case of the real Earth and further proposed that crosscorrelating seismic noise observed at two different receivers located within a heterogenous three-dimensional material will produce the same signal that would be observed at either receiver if it were a seismometer observing an impulse response produced at the location of the other receiver.

Nevertheless, modern seismic interferometry was not actually born until much later papers by Schuster (2001), Lobkis and Weaver (2001), Campillo and Paul (2003), Derode et al. (2003), Wapenaar (2004), and others. In addition, Claerbout's workflow drew mostly upon techniques and principles that were already established. For example, it has been known since the 19th Century (Rayleigh, 1896) that acoustic waves exhibit *reciprocity*, meaning that the waves detected at one location due to a source at a second location would be the same if source and detector were interchanged. Seismic interferometry applies techniques such as crosscorrelation to take advantage of this principle. In addition, it has been recognized since the beginning of the 20th Century (Omori, 1905) that earthquakes originating from the same area often produce similar seismograms. This observation requires strong similarities in source characteristics and/or path properties to a given receiver, which has profound implications for understanding the earthquake source and wave propagation in the subsurface.

Only in recent decades have sufficient theoretical understanding and computational power been available to rigorously exploit Omori's observation for interrogating subsurface structure and source characteristics. Beginning in the 1950s, major advancements were made that led to the development of seismic interferometry. The most notable foundational discoveries were made by Keiiti Aki, Professor of seismology at the Massachusetts Institute of Technology, and his coauthors. Seismic interferometry developed partly out of Aki's (1957) technique of spatial autocorrelation (SPAC), which is the crosscorrelation of a particular signal with itself in the spatial domain. In this case, an earthquake trace is correlated with a trace for the same earthquake collected at another location. Spatial autocorrelation for use characterizing the structure of a medium and the nature of wave propagation within it was introduced to seismology by Aki (1957). Aki defined the SPAC function, $\phi(\xi, t)$, as

$$\phi(\xi, t) = \overline{u(x, t)u(x + \xi, t)}, \tag{7}$$

where $u(x, t)$ is displacement as a function of time and distance, the overbar, $\overline{\cdot}$, denotes a spatial average, and ξ is a distance in the x-location. For two-dimensional plane waves, the SPAC function is expressed as

$$\phi(\xi, \eta, t) \equiv \overline{u(x, y, t)u(x + \xi, y + \eta, t)}, \tag{8}$$

where y is another dimension and η is an offset in that

dimension. In polar coordinates, and assuming that the wave is not polarized and travels at a single speed, the SPAC function defined by Aki (1965) is

$$\phi(r,\lambda) = \overline{u(x,y,t)u(x+r\cos\lambda, y+r\sin\lambda, t)}. \quad (9)$$

Taking the azimuthal average, he obtained

$$\overline{\phi(r,\lambda)} = \frac{1}{2\pi}\int_0^{2\pi} \phi(r,\lambda)\ \mathrm{d}\lambda. \quad (10)$$

Aki (1957) proposed that computing the correlation function of ground motion between seismometers in this manner could enable estimation of the Green functions and dispersion curves for Rayleigh and Love surface waves. The utility of SPAC for this purpose is demonstrated by the relationship between the azimuthal average of the SPAC function and the time spectral density, $\Phi(\omega)$, obtained using a Hankel transform of $\overline{\phi(r)}$:

$$\Phi(\omega) = \frac{\pi\omega}{c^2}\int_0^{\infty} \overline{\phi(r)} J_0\left(\frac{\omega}{c}r\right) r\ \mathrm{d}r \quad (11)$$

$$\overline{\phi(r)} = \frac{1}{\pi}\int_0^{\infty} \Phi(\omega) J_0\left(\frac{\omega}{c}r\right)\ \mathrm{d}\omega, \quad (12)$$

where ω is frequency, c is wave velocity, and J_0 is the zero-order Bessel function. (The zero-order Bessel function is defined as the solution to the equation $x^2\frac{\mathrm{d}^2y}{\mathrm{d}x^2} + x\frac{\mathrm{d}y}{\mathrm{d}x} + x^2y = 0$, which can be expressed in the form $J_0 = \frac{1}{\pi}\int_0^{\infty}\cos\left(-x\sin t\right)\ \mathrm{d}t$.) Allowing the two-dimensional wave to be polarized, the velocity distribution function, $\frac{p(\omega_0,c)}{P(\omega_0)}$, is expressed as

$$\frac{p(\omega_0,c)}{P(\omega_0)} = \frac{\omega_0}{c^3}\int_0^{\infty} \overline{\rho(r,\omega_0)} J_0\left(\frac{\omega_0}{c(\omega_0)}r\right) r\ \mathrm{d}r, \quad (13)$$

where ρ is the autocorrelation coefficient. Surface wave dispersion curves, which depict the degree of observed amplitude reduction as a function of frequency, are used to infer the near-surface elastic properties of a medium, including the S-wave velocity profile.

Aki (1969) and Aki and Chouet (1975) subsequently showed that the seismic coda contains the signal of both surface and body waves backscattered by heterogeneities along their path. As they noted, an implication is that the coda waves contain data that can be used to find the earthquake source spectra. More relevant for the present purposes, however, is that the coda waves might reveal characteristics of the path and, hence, subsurface structure. Not only does the coda wave help reveal the shallow velocity structure through use of dispersion curves, backscattering itself makes possible VSM because scattering causes waves to pass through multiple paths that connect clusters of earthquakes to a single receiver (or single earthquakes to an array of receivers). This helps illuminate areas of interest by dramatically increasing the waves that reach a receiver from an area.

Years later, Spudich and Bostwick (1987) showed that seismograms recorded at a single receiver from a cluster of earthquakes can be used to turn the earthquakes into a virtual array of seismometers using plane-wave decomposition. Using single-seismometer observations from aftershocks of the 1984 Morgan Hill, California, earthquake, Spudich and Bostwick (1987) confirmed the theoretical claim that the positions of sources and receivers are interchangeable. They also showed that, by treating an earthquake cluster as a virtual array, they could determine the general locations and density of scatterers, as well as the initial wave propagation directions. Nevertheless, the methods they employed are different from seismic interferometry because they did not involve crosscorrelation and similar techniques.

Their achievement was based upon the principle of *Green function reciprocity*, which is similar to seismic reciprocity but more specifically states that the Green function (impulse response) will be the same for waves passing from source location to receiver location as from receiver to source. The principle is expressed as

$$G_{ij}\left(\mathbf{x}, t; \mathbf{x}_0, 0\right) = G_{ji}\left(\mathbf{x}_0, t; \mathbf{x}, 0\right), \quad (14)$$

an equation given by Spudich and Bostwick (1987) after Aki and Richards (1980), with symbols as in Equation 3 (see also Sato and Fehler, 2012). An important implication of reciprocity for seismic interferometry is that it enables the use of time reversal for seismological applications. The principle *time reversal* implies that it is irrelevant whether we consider wave propagation moving forward or backward in time or, hence, from source to receiver and *vice versa*, assuming that the medium is lossless (Fink et al., 2000; Fink and Prada, 2001; Bakulin and Calvert, 2006). The use of time reversal is valid because

the seismic wave equation (e.g., Shearer, 2009),

$$\frac{\partial^2 u}{\partial t^2} = c^2 \frac{\partial^2 u}{\partial x^2}, \tag{15}$$

has the same solution if t is positive or negative: $\mathbf{u}(x,t) = f(x \pm ct)$ or $\mathbf{u}(x,-t) = f(x \pm ct)$.

Cassereau and Fink (1992, 1993) later formulated a time-reversed wavefield based upon a two-step conceptual procedure involving a primary wave source and mirrors at the boundaries of the medium that act as a secondary source. In the first step, the primary source emits a signal (in the case of their study, the signal is a pressure pulse) that is detected at all points on the mirrors. In the second step, the primary source is removed immediately after transmitting the signal, and the mirrors become *secondary sources*, transmitting the time-reversed pressure signal (both monopole and dipole) that they detected at each point earlier back into the medium. The authors' equation for the time-reversed pressure field observed at a given location $\mathbf{x}$ and time t, and expressed for convenience in the notation of Curtis et al., 2009 (coordinate system notation slightly modified from above), is

$$P_{TR}(\mathbf{x},t) = \oint_S \frac{1}{\rho} \left[G\left(\mathbf{x},t|\mathbf{x}'\right) \star \nabla' P\left(\mathbf{x}',-t\right) - P\left(\mathbf{x}',-t\right) \star \nabla' G\left(\mathbf{x},t|\mathbf{x}'\right) \right] \cdot \mathbf{n}\, \mathrm{d}\mathbf{x}', \tag{16}$$

with $P(\mathbf{x}',-t)$ the time-reversed pressure field, $\nabla' P(\mathbf{x}',-t)$ the gradient of the time-reversed pressure field, S the boundary (as in Figure 1), t the time since the signal was radiated from the boundary, $G(\mathbf{x},t|\mathbf{x}')$ the Green function in the medium (in their case, an acoustic medium), $\nabla' G(\mathbf{x},t|\mathbf{x}')$ the gradient of the Green function, $\mathbf{x}'$ referring to a location that is the mirror of $\mathbf{x}$ across the boundary, ρ the medium density, $\mathbf{n}$ the normal to the boundary, and $\star$ here represents convolution (similar in practice to crosscorrelation). This derivation became useful for seismic interferometry, and especially for VSM, because it provides a rigorous way to treat virtual sources located at the boundaries of a complex, three-dimensional medium, which is an obvious analogue to seismological observations made at the surface of the Earth. This formulation will be applied when presenting the theoretical framework for VSM in Section III-C1.

B. Seismic interferometry: The foundation for virtual seismometers

The term *seismic interferometry*, which was coined by Schuster (2001), has traditionally involved the use of crosscorrelation of seismograms obtained at different receivers to estimate path and source properties—especially the Green functions—between the receivers and, hence, to construct *virtual sources* (Wapenaar et al., 2010). A virtual source is the location of a receiver that crosscorrelation permits imagining as a source (Schuster, 2001; Bakulin and Calvert, 2004, 2006; Wapenaar et al., 2010). Using this approach, it is possible to determine the seismic trace that would be observed at another receiver due to waves transmitted from the virtual source.

The crosscorrelation function at the heart of seismic interferometry computes the *coherence*, or similarity, between multiple signals. Crosscorrelation finds the difference in travel time of recorded arrivals from the same source(s) at different receivers (Curtis et al., 2006). The resulting crosscorrelelogram, C, is expressed by

$$C(\tau) \equiv \int_0^T p_2(t+\tau) p_1(t)\, \mathrm{d}t, \tag{17}$$

where t is time, T is integration time window, and τ is a time offset (Snieder, 2004). The wavefields at receivers 1 and 2 are given by p_1 and p_2, respectively, with

$$p_{1,2}(t) = \sum_s S_s \frac{\left(t - \frac{r_{1,2}^{(2)}}{c}\right)}{r_{1,2}^{(s)}}, \tag{18}$$

where S_s is the signal S emitted from scatterer number s and $r_{1,2}$ represents the distance from a given scatterer to receivers 1 and 2, respectively. Plugging Equation 18 into Equation 17, we find an expanded expression for the crosscorrelelogram of signals from two receivers:

$$C(\tau) = \sum_{s,s'} \int_0^T S_s(t) S_s(t+\tau)\, \mathrm{d}t, \tag{19}$$

where $\sum_{s,s'}$ is the double sum over all scatterers.

The crosscorrelelogram derived from seismic traces from two nearby receivers produces the ballistic Green function between the receivers, even though energy from neither trace may have actually traveled ballistically from one point to the other (e.g., Lobkis and Weaver, 2001;

Weaver and Lobkis, 2001; Campillo and Paul, 2003; Derode et al., 2003; Roux and Fink, 2003; Wapenaar, 2004; Wapenaar and Fokkema, 2006). Snieder (2004) confirmed this relationship mathematically by deriving an expression for the crosscorrelelogram of scalar waves in three dimensions:

$$C(\omega) = 8\pi^2 \overline{\left|S(\omega)^2\right|} \left(\frac{c}{i\omega}\right) \times \left(-\frac{e^{ikR}}{4\pi R}\int_{-\infty}^{0} n\,\mathrm{d}x - \frac{e^{-ikR}}{4\pi R}\int_{-\infty}^{0} n\,\mathrm{d}x\right), \tag{20}$$

where n is the scatterer density, k is the wavenumber, and R is the distance between receivers 1 and 2. The Green function for waves propagating from receiver 1 to receiver 2 (the retarded Green function) is given by the term $-\frac{e^{ikR}}{4\pi R}$, and the Green function that arises from waves propagating from receiver 2 to receiver 1 (the advanced Green function) is given by $-\frac{e^{-ikR}}{4\pi R}$. This relationship can be simplified by assuming a constant n and resolving the integrals, leaving

$$C(\omega) = 8\pi^2 \overline{|S(\omega)|^2} \left(\frac{ncL}{i\omega}\right) \times \left(-\frac{e^{ikR}e^{-\frac{R}{2L}}}{4\pi R} - \frac{e^{-ikR}e^{-\frac{R}{2L}}}{4\pi R}\right), \tag{21}$$

where L is the attenuation length in the medium, and the two terms inside the last set of brackets represent the retarded and advanced Green functions, respectively.

For *surface* waves in a three-dimensional elastic medium, Snieder (2004) showed a somewhat different relationship (here in indicial notation):

$$C_{ij}(\omega) = \pi \sum_m \overline{|S^m(\omega)|^2} n c_m L_m \times \left\{\frac{G_{ij}^m(\mathbf{r}_2,\mathbf{r}_1)}{i\omega} + \frac{G_{ij}^m(\mathbf{r}_1,\mathbf{r}_2)}{i\omega}\right\}, \tag{22}$$

where c_m and L_m are the wave speed and attenuation length, respectively, of surface mode m. The total, far-field, surface-wave Green function, G_{ij}, is the sum of the surface-wave Green functions of all modes, as in $G_{ij}(\mathbf{r},\mathbf{r}_0) = \sum_m G_{ij}^m(\mathbf{r},\mathbf{r}_0)$, where

$$G_{ij}^m(\mathbf{r},\mathbf{r}_0) = p_i^m(z,\phi) p_j^{m*}(z_0,\phi) \frac{e^{i\left(k_m R + \frac{\pi}{4}\right)}}{\sqrt{\frac{\pi}{2}k_m R}}, \tag{23}$$

and where z is the depth within a layered medium, z_0 is the reference depth, and ϕ is the azimuth between unit vector points $\mathbf{r}$ and $\mathbf{r}_0$ for transversely polarized waves.

The use of crosscorrelation to generate the signals that would be transmitted by virtual sources gained wide appeal and utility after Campillo and Paul (2003) demonstrated using real data that "noise" within the coda contains coherent signal that can be used to describe the elastic properties of the medium between receivers, including obtaining the surface wave Green function. With sufficient azimuthal coverage of earthquakes around the receivers, crosscorrelation of the coda signal observed at each sensor can yield the seismogram that would be expected at one receiver if a second receiver were instead an earthquake. This technique of crosscorrelating signals obtained at two receivers to obtain the Green function describing the response that would be detected at one receiver from an impulse generated at the other falls within the realm of *passive imaging* because it does not require that an actual signal be emitted from the virtual source location. Most seismic interferometry conducted thus far has made use of data contained within surface waves, rather than body waves (Curtis et al., 2009).

Since 2003, passive imaging using seismic interferometry on the ASF has been employed extensively to estimate subsurface characteristics, and numerous methodological improvements have been made, as summarized by Curtis et al. (2006). For example, Snieder (2004) presented a derivation for obtaining the Green function from crosscorrelated coda waves that does not rely upon an assumption that the normal modes of the system experience equipartitioning and are uncorrelated. The initial work by Campillo and Paul (2003) had made the simplifying assumption that the Earth's normal and surface wave modes experience *equipartitioning*, meaning that the energy field is distributed evenly in space, in this case between different modes (Snieder et al., 2010). It has been proposed that equipartitioning of seismic wave energy can result from multiple scattering in the subsurface (Hennino et al., 2001). However, the assumption of equipartitioning for surface wave modes is not strictly true because the fundamental (lowest frequency) modes for both Love and Rayleigh surface

waves usually contain more energy than the sum of all of the higher modes (Snieder, 2004). In addition, Snieder (2004) observed that the assumption of equipartitioning of the Earth's normal modes that was made by Campillo and Paul (2003) was not valid in their case because they used ground motion records with durations less than the time needed for a P-wave to propagate once to the other side of the Earth, and he provided theoretical solutions to this problem in future work. Finally, early seismic interferometry, including that of Snieder (2004), required that the wavefield be fully diffuse. The reliance upon this rigid assumption was relaxed by Wapenaar (2004), who presented a method for obtaining the Green function between receivers within any type of inhomegenous, elastic medium using crosscorrelation, provided that the receivers are both placed on a free surface (e.g., the surface of the Earth).

Shortly after the seminal work by Campillo and Paul (2003), Sabra et al. (2005) and Shapiro et al. (2005) used the impulse response (Green function) from crosscorrelations of microseisms and/or the ASF to conduct surface-wave tomography between stations in southern California. This early study showed that reasonable surface wave velocities can be extracted from seismic interferometry in an area where the rock types and their expected seismic velocities are reasonably well known. Many subsequent studies have conducted surface-wave ambient noise tomography (ANT), including a wide-band (10–50 s) Rayleigh wave ANT study across nearly the whole of Europe that enabled estimation of regional sedimentary basin and crustal thicknesses, which the authors (Yang et al., 2007) claimed represented a substantial improvement upon traditional seismic tomography techniques. Prieto et al. (2011) later demonstrated that seismic interferometric methods can be used to estimate not only the Green functions but also to extract information about amplitudes of waves within the ambient seismic field, which can reveal details about the subsurface attenuation and amplification characteristics.

C. Virtual seismometers

One of the most consequential developments in the field of seismic interferometry was the development by Curtis et al. (2009) of the technique of *virtual seismometry* (VSM), which is something of the reverse of traditional passive imaging in that it permits estimation of the Green function between two nearby *earthquakes*, rather than two receivers (Figure 1). Similar to more traditional methods of seismic interferometry that involve constructing virtual *sources*, this technique removes the effects of the source and receiver, permitting estimation solely of the parameters of the ray path (Curtis et al., 2009; Matzel et al., 2015, 2016). This technique is enticing in part because it can enhance seismic imaging studies, particularly where seismometer networks are absent, such as in oceanic areas or in the subsurface.

1) Theory: VSM shares much of its theoretical background with traditional seismic interferometry, including applying crosscorrelation (or convolution) to seismic signals or noise. More specifically, Curtis et al. (2009) based their theoretical explanation for VSM upon work by Cassereau and Fink (1992, 1993), who used convolution to relate the Green function of a medium to the time-reversed pressure field (Equation 16). Curtis et al. (2009) applied those authors' conceptual model of a primary source within a medium surrounded by sensors on the exterior that also act as secondary sources that transmit a time-reversed signal. Using this framework, together with equations derived by Wapenaar (2004), Wapenaar and Fokkema (2006), and van Manen et al. (2005, 2006), Curtis et al. (2009) found the following expression for the Green function (and its time-reverse equivalent) between a source $\mathbf{x}_1$ and an observation point $\mathbf{x}_2$:

$$\begin{aligned} &G\left(\mathbf{x}_2, t|\mathbf{x}_1\right) - G\left(\mathbf{x}_2, -t|\mathbf{x}_1\right) \\ &= \oint_S \frac{1}{\rho}\left[G\left(\mathbf{x}_2, t|\mathbf{x}'\right) * \nabla' G\left(\mathbf{x}', -t|\mathbf{x}_1\right) - \right. \\ &\left. \nabla' \, G\left(\mathbf{x}_2, t|\mathbf{x}'\right) * G\left(\mathbf{x}', -t|\mathbf{x}_1\right)\right] \cdot \mathbf{n} \, \mathrm{d}\mathbf{x}'. \end{aligned} \tag{24}$$

Here, $G_{ij}\left(\mathbf{x}_1, t|\mathbf{x}'\right)$ refers to the Green function at position $\mathbf{x}_1$ given a source at position $\mathbf{x}'$. The i index describes the spatial component of particle displacement at the $\mathbf{x}_1$ location, and the j index describes the spatial component of a unidirectional point source applied at the source location $\mathbf{x}'$. As before, $\mathbf{x}'$ is a location that is the mirror of $\mathbf{x}$ with respect to the medium boundaries.

Invoking source-receiver reciprocity, $G\left(\mathbf{x}', t|\mathbf{x}_1\right) =$

$G(\mathbf{x}_1, t|\mathbf{x}')$, Curtis et al. (2009) slightly modified the preceding equation such that it relies only upon sources on the boundary of the medium, which permits estimation of the Green function between points $\mathbf{x}_1$ and $\mathbf{x}_2$:

$$\begin{aligned} &G(\mathbf{x}_2, t|\mathbf{x}_1) - G(\mathbf{x}_2, -t|\mathbf{x}_1) \\ &= \oint_S \frac{1}{\rho} \left[G(\mathbf{x}_2, t|\mathbf{x}') * \nabla' G(\mathbf{x}_1, -t|\mathbf{x}') - \right. \\ &\left. \nabla' G(\mathbf{x}_2, t|\mathbf{x}') * G(\mathbf{x}_1, -t|\mathbf{x}') \right] \cdot \mathbf{n} \, \mathrm{d}\mathbf{x}'. \end{aligned} \tag{25}$$

Following van Manen et al. (2005, 2006, 2007), Curtis et al. (2009) then converted Equation 25 (heretofore given for an acoustic medium) into an elastic formulation:

$$\begin{aligned} &G(\mathbf{x}_2, -t|\mathbf{x}_1) - G(\mathbf{x}_2, t|\mathbf{x}_1) \\ &= \oint_S \left[G_{in}(\mathbf{x}_2, t|\mathbf{x}') * n_j c_{njkl} \partial'_k G_{ml}(\mathbf{x}_1, -t|\mathbf{x}') - \right. \\ &\left. n_j c_{njkl} \partial'_k G_{il}(\mathbf{x}_2, t|\mathbf{x}') * G_{mn}(\mathbf{x}_1, -t|\mathbf{x}') \right] \mathrm{d}\mathbf{x}', \end{aligned} \tag{26}$$

with c_{ijkl} the elastic stiffness tensor, n_i the components of the normal vector to the boundary S, $G_{ij}(\mathbf{x}_1, t|\mathbf{x}')$ the Green tensor defined with i indicating the component of particle displacement given a point source oriented in the j direction, and ∂_k representing the partial derivative in the k direction. This equation relates to impulses generated at location $\mathbf{x}'$, which is located on the surface S, and measured at points $\mathbf{x}_1$ and $\mathbf{x}_2$ (as in Figure 1). The signals are conceptualized as unidirectional impulses fired in each of the three directions j. Using Green function reciprocity and this formulation, Curtis et al. (2009) presented the following equation to find the Green function directly:

$$\begin{aligned} &G_h^{im}(\mathbf{x}_2, t|\mathbf{x}_1) \\ &= -\oint_S \left[\tilde{G}_{ni}(\mathbf{x}', t|\mathbf{x}_2) * n_j c_{njkl} \partial'_k \tilde{G}_{lm}(\mathbf{x}', -t|\mathbf{x}_1) - \right. \\ &\left. n_j c_{njkl} \partial'_k \tilde{G}_{li}(\mathbf{x}', t|\mathbf{x}_2) * \tilde{G}_{mn}(\mathbf{x}', -t|\mathbf{x}_1) \right] \mathrm{d}\mathbf{x}'. \end{aligned} \tag{27}$$

Converting from time to frequency, they obtained

$$\begin{aligned} &G_{im}^h(\mathbf{x}_2|\mathbf{x}_1) \\ &= -\oint_S \left[\tilde{G}_{ni}(\mathbf{x}'|\mathbf{x}_2) * n_j c_{njkl} \partial'_k \tilde{G}_{lm}(\mathbf{x}'|\mathbf{x}_1) - \right. \\ &\left. n_j c_{njkl} \partial'_k \tilde{G}_{li}(\mathbf{x}'|\mathbf{x}_2) * \tilde{G}_{mn}(\mathbf{x}'|\mathbf{x}_1) \right] \mathrm{d}\mathbf{x}', \end{aligned} \tag{28}$$

where $G_{im}^h(\mathbf{x}_2|\mathbf{x}_1) = G_{im}(\mathbf{x}_2|\mathbf{x}_1) - G_{im}^*(\mathbf{x}_2|\mathbf{x}_1)$ is the homogeneous Green function between the two sources, $\mathbf{x}_1$ and $\mathbf{x}_2$, and where the * superscript denotes the complex conjugate. The right-hand side of this latter equation prescribes crosscorrelation in the time domain. Overall, as noted by Curtis et al. (2009), this equation permits estimating the signal that would have been recorded at location $\mathbf{x}_2$ if it were instead a receiver.

Although Equation 28 applies to the elastic case (which requires input from three unidirectional impulses), Curtis et al. (2009) also provided an analogous equation for the acoustic case, which is excluded here for brevity. Despite its value, Equation 28 is not presented in a format that honors source signatures $W_1(\omega)$ and $W_2(\omega)$, which might be produced from sources $\mathbf{x}_1$ and $\mathbf{x}_2$, respectively. The Green functions resulting from these source profiles is equal to the homogeneous Green function convolved with the crosscorrelation of the two source signatures:

$$\begin{aligned} &W_2 W_1^* G_{im}^h(\mathbf{x}_2|\mathbf{x}_1) \\ &= -\oint_S \left[\tilde{G}_{ni}(\mathbf{x}'|\mathbf{x}_2) \, n_j c_{njkl} \partial'_k \tilde{G}_{lm}(\mathbf{x}'|\mathbf{x}_1) - \right. \\ &\left. n_j c_{njkl} \partial'_k \tilde{G}_{li}(\mathbf{x}'|\mathbf{x}_2) \, \tilde{G}_{mn}(\mathbf{x}'|\mathbf{x}_1) \right] \mathrm{d}\mathbf{x}'. \end{aligned} \tag{29}$$

Although this expression is given in terms of source signatures, it is not in the form of moment tensors, making rendering it difficult to use for natural earthquakes. This is remedied by modifying the previous equation to

$$\begin{aligned} &M_{ip}^2 M_{mq}^1 G_{im}^h(\mathbf{x}_2|\mathbf{x}_1) \\ &= \int_S \left[M_{ip}^2 \partial_p \tilde{G}_{ni}(\mathbf{x}'|\mathbf{x}_2) \, n_j c_{njkl} \partial'_k \tilde{G}_{lm}^*(\mathbf{x}'|\mathbf{x}_1) - \right. \\ &\left. n_j c_{njkl} \partial'_k M_{ip}^2 \partial_p \tilde{G}_{li}(\mathbf{x}'|\mathbf{x}_2) \, M_{mq}^1 \partial_q \tilde{G}_{nm}^*(\mathbf{x}'|\mathbf{x}_1) \right] \mathrm{d}\mathbf{x}', \end{aligned} \tag{30}$$

where M^1 and M^2 are the moment tensors from earthquakes located at $\mathbf{x}_1$ and $\mathbf{x_2}$, respectively. In addition, the term $n_j c_{njkl} \partial'_k M_{mq}^1 \partial_q \tilde{G}_{lm}(\mathbf{x}'\mathbf{x}_1)$ is equal to $T_n(\mathbf{x}'|\mathbf{x}_1)$, the n^{th} orientation component of traction. Substituting, we obtain

$$\begin{aligned} &M_{ip}^2 M_{mq}^1 G_{im}^h(\mathbf{x}_2|\mathbf{x}_1) \\ &= \int_S \left[u_n(\mathbf{x}'|\mathbf{x}_2) \cdot T_n^*(\mathbf{x}'|\mathbf{x}_1) - \right. \\ &\left. T_n(\mathbf{x}'|\mathbf{x}_2) \cdot u_n^*(\mathbf{x}'|\mathbf{x}_1) \right] \mathrm{d}\mathbf{x}'. \end{aligned} \tag{31}$$

These derivations show that the virtual seismometer actually measures strain, which provides this technique with certain advantages that will be discussed below. However, for compatibility with the record produced from a conventional particle-displacement seismometer, the authors convert the previous equation into terms of particle displacement (u) and velocity ($\dot{u}$), removing terms of traction, T_n:

$$M_{ip}^2 M_{mq}^1 \partial_p \partial_q' G_{im}^h \left(\mathbf{x}_2|\mathbf{x}_1\right) = ik\omega \int_s u_n \left(\mathbf{x}'|\mathbf{x}_2\right) u_n^* \left(\mathbf{x}'|\mathbf{x}_1\right) \mathrm{d}\mathbf{x}', \tag{32}$$

where K is a constant.

The final expression for the moment tensor-modified Green function, as obtained from input velocity seismograms and expressed in indicial notation, is

$$M_{ip}^2 M_{mq}^1 \partial_p \partial_q' G_{im}^h \left(\mathbf{x}_2|\mathbf{x}_1\right) = -\frac{K}{i\omega} \int_s \dot{u}_n \left(\mathbf{x}'|\mathbf{x}_2\right) \dot{u}_n^* \left(\mathbf{x}'|\mathbf{x}_1\right) \mathrm{d}\mathbf{x}'. \tag{33}$$

2) Steps to build a virtual seismometer: On the basis of the preceding theoretical discussion, several steps are followed to create a "virtual seismometer," which resemble the steps needed to conduct traditional seismic interferometry. First, time-series seismic data are obtained for two or more earthquakes in an area. Data can be downloaded from sources such as the Wilber 3 web service (Newman et al., 2013) provided by the Incorporated Research Institutes for Seismology (IRIS), and imported locally using software including Standing Order for Data, SOD (Owens et al., 2004). It is also necessary to identify pairs of earthquakes from the selected dataset that roughly form a straight line to a receiver, as illustrated in Figure 1c. This is because the region of constructive interference associated with the signal observed at two receivers due to an arrival from a given scatterer lies in the line connecting the two receivers (Snieder, 2004). Consequently, Curtis et al. (2009) noted that the Green function between two virtual seismometers ($\mathbf{x}_1$ and $\mathbf{x}_2$) can only be determined in a cone-shaped zone around the outward extension of the line connecting those two events (Figure 1c). Seismic waveforms containing both one and three components have been successfully applied to this technique (e.g., Curtis et al., 2009). Next, these data are filtered using software such as the Seismic Analysis Code, SAC, a command-line toolbox for seismological signal processing and analysis of time-series data (Goldstein et al., 2003; Helffrich et al., 2013). In the case of the original study by Curtis et al. (2009), the seismic data were bandpass filtered to include only the 15–33 s period range. The authors provide no other information about their filtering choices but, presumably, the signals were filtered to deconvolve instrument responses. Subsequently, the waveforms detected for each pair of events ($\mathbf{x}_1$ and $\mathbf{x}_2$) at the aligned detector are crosscorrelated. In practice, crosscorellation and other standard seismological techniques can be efficiently conducted using software such as msNoise, a Python-based application that provides tools for conducting seismic interferometry and is tailored to the use of the ASF (Lecocq et al., 2014). Within the msNoise software, the crosscorrelelograms are then stacked (summed) between each pair of events and, finally, the Green functions are found to describe the impulse response between event pairs.

3) Applications and uses of VSM*:* VSM is only eight years old and has not found a large array of applications in practical imaging studies. The article by Curtis et al. (2009) has been cited approximately 80 times, according to metrics by Google Scholar, and most of these citations appear to be for seismic interferometry methods development papers. However, the applications of this technique outside strict methods development have been diverse, ranging from imaging the subduction zone interface to obtaining moment tensors of microseismic events. As noted previously, a key advantage of this method over previous seismological techniques is that it enables extraction of source and path parameters from areas that might previously have escaped interest due to their large distances from seismic observation networks.

In their original paper, Curtis et al. (2009) provided a sample application of their new technique by creating virtual seismometers in the Alaskan subduction zone and beneath the western USA (Figure 2). Each pair of earthquakes used to construct the virtual seismometer was observed by a handful of real seismometers distributed in a cone shape surrounding the extension of the line connecting the earthquakes. The authors used each virtual

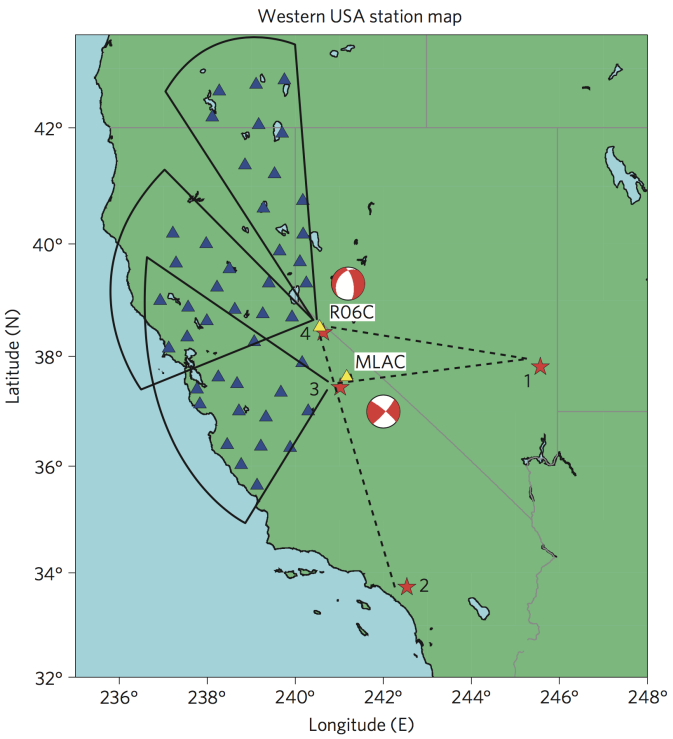

Fig. 2: Map of the stations and earthquake locations used by Curtis et al. (2009) for constructing virtual seismometers. Blue triangles are seismometers used for the interferometry, red stars are earthquakes, yellow triangles are seismometers located near the earthquakes that were used to validate the virtual seismic traces, and solid black lines bound regions of receivers used to construct virtual seismometers for each earthquake pair. Black dashed lines connect pairs of earthquakes used to construct virtual seismometers (earthquakes 3 and 4).

seismometer to estimate the seismic response (not simply the Green function) that would have been recorded at its location had it been a seismometer observing the other earthquake in its pair. This was shown for both a strike-slip and a normal faulting source. For validation purposes, they compared the virtual signal for the observed earthquake with the real response measured by a seismometer located close to the virtual seismometer. In an additional test, the authors used the signal from the 2008 Sichuan, China, earthquake that reached their study locations in the western USA and near Alaska. They compared the results obtained from real seismometers to the signal that would be detected if nearby virtual seismometers recorded the Sichuan earthquake, and they found a reasonably good match in both cases.

Matzel et al. (2014, 2015, 2016) and Morency and Matzel (2017) applied VSM to microseismic data from enhanced geothermal systems, including to monitoring for induced seismic hazards. The studies by Matzel et al. (2014, 2015) constructed virtual seismometers from events within a microseismic cloud to improve information about the size, location, and source characteristics of the events, including their temporal evolution. Morency and Matzel (2017) were able to use this technique to conduct moment tensor inversion on microseismic events located within a region near the Newberry Volcano, Oregon, that experienced induced microseismicity due to fluid injection for enhanced geothermal production. Taking advantage of the observation that the crosscorrelated signal of the wavefield from two earthquakes measured at the surface is the product of a moment tensor with the strain field resulting between the sources, they inverted for the moment tensors themselves.

Intriguingly, Matzel et al. (2015) also conducted a proof-of-concept study to characterize the Blanco oceanic transform zone, a plate boundary located offshore Oregon, USA. The authors obtained the Green function between some 40 earthquakes and showed subtle differences between the resulting Green function waveform and what would have been obtained synthetically using the University of Colorado, Boulder, 3D Earth Model. They claimed that these differences arise from their study having captured subtle structural characteristics of the fault system.

Melo and Malcolm (2011) and Melo et al. (2012) used VSM to improve microearthquake locations and enhance local velocity models by comparing event locations using travel-time estimates made from virtual seismometers. Their travel-time estimates are derived from Green functions between microearthquakes (one source and one virtual seismometer) estimated using VSM. These authors reported that their interferometric event location comparison technique was successful and superior in some aspects to techniques relying upon traditional seismology and velocity models.

In novel studies, Liu et al. (2015, 2016) applied VSM to the field of "seismic-while-drilling." These authors crosscorrelated drill-bit noise from different locations within a wellbore, a technique that has been applied by others in recent years to estimate path parameters in an oil and gas setting. This technique benefits from the

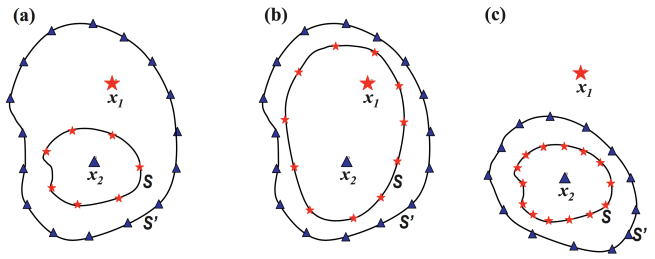

Fig. 3: Schematic maps given by Curtis and Halliday (2010) to illustrate geometries of (virtual) sources and (virtual) receivers that can be employed by their method of source-receiver interferometry. Triangles are receivers and stars are sources. In three dimensions, the lines labeled S and S' would be closed surfaces.

drill bit being a seismic energy source whose location is known exactly and is close to the medium of interest. Seismic-while-drilling, including the studies by by Liu et al. (2015, 2016), requires making assumptions or estimates of the drill-bit noise signature. In the new applications by Liu and colleagues, the drill-bit noise was converted to a set of virtual seismometers, which enabled them to obtain virtual reflection images of parts of the medium beneath the borehole. The authors redatumed the retrieved reflections to the known borehole depth using interferometric methods, which enabled them to avoid having to rely upon an uncertain velocity model of the overlying strata to obtain depths of the imaged reflections below. Their work showed a substantially improved image of reflections immediately below the borehole.

Most notably, the development of VSM has assisted with the marked advance in seismic interferometry techniques of the past several years. Just one year after Curtis et al. (2009) published their paper on VSM, Curtis and Halliday (2010) built upon the technique of VSM (which they referred to as *inter-source interferometry* [Figure 1a], as opposed to the more traditional *inter-receiver interferometry* [Figure 1c]) to develop a third form of seismic interferometry that they dubbed *source-receiver interferometry* (Figure 3). In the latter method, Green functions and seismograms can be estimated between a (virtual) source and a (virtual) receiver, rather than simply between sources or receivers. The derivations used to develop source-receiver interferometry united the various interferometric methods that relied upon crosscorrelation and convolution into a single theoretical framework that provided practitioners with the ability to draw from the power of both related techniques. Source-receiver interferometry markedly expanded the practical applications of seismic interferometry *sensu lato* because it allowed for the use of much more varied source-receiver geometries. Previously, inter-source interferometry relied upon a (loose in practice) requirement that sources completely surrounded the medium under study (Figure 1c), although this requirement could be relaxed in numerous ways, including in the presence of many scatterers that help to better illuminate the medium, and in the event of a free surface along the boundary, as described above (see Lobkis and Weaver, 2001; Curtis et al., 2006; Wapenaar and Fokkema, 2006; Poliannikov, 2011). Even as it provided new capabilities for interrogating the paths between sources and/or receivers, source-receiver interferometry added its own geometric requirements, namely that both a shell of receivers and of sources bound the medium under study (Figure 3), although these shells can be composed of two-dimensional rings of sources and receivers placed at the Earth's surface. Recognizing geometric limitations for illuminating structures in certain locations during interferometric reflection imaging studies, Poliannikov (2011) provided enhancements that allowed redatuming a structure from areas of low-illumination to areas of high illumination within a medium, even when the ideal source or receiver geometries for source-receiver interferometry are not fully met.

Poliannikov et al. (2012) took advantage of the recent developments within all three branches of seismic interferometry to image the top of a subducting slab using earthquakes occurring there. These authors estimated the Green function between pairs of earthquakes occurring near the difficult-to-image subduction interface using a multi-step method: First, they applied classical (inter-receiver) interferometry to conceptualize (redatum) earthquakes occurring within the subduction zone as being virtual sources at the surface, occurring near the recording array. In the process of redatuming the subduction zone earthquakes, their method also redatumed multiples associated with the interface itself up to the surface. In the second step, the authors applied source-receiver interferometry to redatum these surface reflections back

into the subduction zone, hence providing something like a reflection image of the interface. Although not a strict use of VSM, this application illustrates the ways that the method has launched conceptual and practical advancements that have broadened the use of seismic interferometry. Following the development of the related technique of source-receiver interferometry (Curtis and Halliday, 2010), studies have often applied VSM in concert with other forms of seismic interferometry. Most likely, the broader field of seismic interferometry will advance through the routine use of a combination of the three related methods, rather than strict reliance of one type.

IV. Conclusions: The promise of virtual seismometers

VSM is new, and its broad applicability within and beyond seismology virtually ensures that many important contributions will arise from it in the coming years. Above, I have presented several ways in which the technique has already been applied to geoscience questions. However, this method has thus far received much more interest in the context of seismic interferometry methods development than in terms of practical applications. Given its considerable potential to illuminate source and path parameters, including in areas with limited seismometer coverage or in cases of microseismicity, its most fruitful applications may prove to be in:

1) *Unconventional oil and gas reservoirs and enhanced geothermal fields.* As Matzel et al. (2014, 2015, 2016) have shown, VSM can reveal the change in source mechanisms over time and can help illuminate faults from within the microseismic cloud in geothermal fields. These same capabilities can be applied to unconventional oil and gas settings.
2) *Areas experiencing triggered seismicity.* The capacity of this method to virtually place a seismometer within a cloud of seismicity provides somewhat unique capabilities for the study of induced and triggered seismicity. First, the sensitivity of this method to the source mechanism could allow rapid determination of the moment tensors of active seismicity, which could reveal the orientations of active faults around which injection should be avoided in the ambient seismic field (see, e.g., Lund Snee and Zoback, 2016; Walsh and Zoback, 2016). In addition, this technique might improve catalogue completeness for small earthquakes and provide better earthquake locations, which could reveal aligned groups of events that define active faults. Schoenball and Ellsworth (2017) recently demonstrated the merits of using event relocations for identifying fault planes in areas experiencing induced seismicity. These authors employed conventional seismology techniques codified in the HYPOINVERSE-2000 (Klein, 2014) and hypoDD (Waldhauser and Ellsworth, 2000) software. Melo and Malcolm (2011) and Melo et al. (2012) demonstrated that VSM might further enhance efforts to relocate seismicity and to identify small faults not detected using conventional methods, particularly in areas with few seismometers or with small earthquakes (Matzel et al., 2014, 2015).
3) *Seismic imaging of remote areas, including beneath oceans.* One of the main advantages of VSM is that it may enable estimation of the Green function and source parameters in areas far from seismometer arrays, but where earthquakes have occurred of sufficient magnitude to be detected at distant arrays. Hence, this method may could provide new capabilities for characterizing seismically active but poorly imaged areas such as mid-ocean ridges and transform zones.

In addition to these specific applications, the method has capabilities that could help advance numerous other types of inquiry. The results of VSM are especially sensitive to source parameters and the structure of the source region, which provides an opportunity to interrogate fault zones far from seismometers (Matzel et al., 2016). An additional advantage of this method is that its formulation is sensitive to the subsurface strain field (Curtis et al., 2009). Hence, this technique may prove to be useful for observing and predicting stress triggering from earthquakes and other stress-strain interactions. VSM, together with the related technique of source-receiver interferometry, is a topic of great potential utility for

geoscientists of many types. Unfortunately, these methods have not yet been used by many practitioners outside the community of seismologists engaged in development of interferometric methods. The somewhat slow adoption of these tools may be a consequence of their newness and the rapid continued development of seismic interferometry, which together may contribute to a scarcity of tools of practical and easy use by non-specialists. Hence, VSM and other emerging forms of seismic interferometry require the development of software programs, proof-of-concept papers, and tutorials that are readily accessible by geoscientists who could put the techniques to work in novel applications.

V. Acknowledgments

I gratefully acknowledge William L. Ellsworth, Gregory C. Beroza, and Alexander R. Blanchette for pointing me toward useful resources and for conversations that helped me frame and advance my thinking about this topic.

References

Aki, K., 1957, Space and time spectra of stationary stochastic waves, with special reference to microtremors: Bulletin of the Earthquake Research Institute, v. 35, p. 415–457, doi:http://hdl.handle.net/2261/11892.

Aki, K., 1965, A note on the use of microseisms in determining the shallow structure of the Earth's crust: GEOPHYSICS, v. 30, no. 4, p. 665–666, doi:10.1190/1.1439640.

Aki, K., 1969, Analysis of the seismic coda of local earthquakes as scattered waves: Journal of Geophysical Research, v. 74, no. 2, p. 615–631, doi:10.1029/JB074i002p00615.

Aki, K., 1980, Scattering and attenuation of shear waves in the lithosphere: Journal of Geophysical Research, v. 85, no. B11, p. 6496, doi:10.1029/JB085iB11p06496.

Aki, K., and Chouet, B., 1975, Origin of coda waves: Source, attenuation, and scattering effects: Journal of Geophysical Research, v. 80, no. 23, p. 3322–3342, doi:10.1029/JB080i023p03322.

Aki, K., and Richards, P.G., 1980, Quantative seismology: Theory and methods: New York, NY, 801 p.

Bakulin, A., and Calvert, R., 2004, Virtual source: new method for imaging and 4D below complex overburden: SEG Technical Program Expanded Abstracts 2004, , no. October, p. 2477–2480, doi:10.1190/1.1845233.

Bakulin, A., and Calvert, R., 2006, The virtual source method: Theory and case study: Geophysics, v. 71, no. 4, p. SI139, doi:10.1190/1.2216190.

Campillo, M., and Paul, A., 2003, Long-Range Correlations in the Diffuse Seismic Coda: Science, v. 299, no. 5606, p. 547–549, doi:10.1126/science.1078551.

Cassereau, D., and Fink, M., 1993, Focusing with Plane Time-Reversal Mirrors - an Efficient Alternative to Closed Cavities: Journal of the Acoustical Society of America, v. 94, no. 4, p. 2373–2386, doi:10.1121/1.407457.

Cassereau, D., and Fink, M., 1992, Time-reversal of ultrasonic fields. III. Theory of the closed time-reversal cavity: IEEE Transactions on Ultrasonics, Ferroelectrics and Frequency Control, v. 39, no. 5, p. 579–592, doi:10.1109/58.156176.

Claerbout, J.F., 1968, Synthesis of a Layered Medium From Its Acoustic Transmission Response: Geophysics, v. 33, no. 2, p. 264–269, doi:10.1190/1.1439927.

Curtis, A., Gerstoft, P., Sato, H., Snieder, R., and Wapenaar, K., 2006, Seismic interferometry – turning noise into signal: The Leading Edge, v. 25, p. 1082–1092, doi:10.1190/1.2349814.

Curtis, A., and Halliday, D., 2010, Source-receiver wave field interferometry: Physical Review E - Statistical, Nonlinear, and Soft Matter Physics, v. 81, no. 4, doi:10.1103/PhysRevE.81.046601.

Curtis, A., Nicolson, H., Halliday, D., Trampert, J., and Baptie, B., 2009, Virtual seismometers in the subsurface of the Earth from seismic interferometry: Nature Geoscience, v. 2, no. 10, p. 700–704, doi:10.1038/ngeo615.

Derode, A., Larose, E., Campillo, M., Fink, M., and Fink, M., 2003, How to estimate the Green's function of a heterogeneous medium between two passive sensors? Application to acoustic waves: Applied Physics Letters, v. 83, no. 15, p. 3054–3056, doi:10.1063/1.1617373.

Fink, M., Cassereau, D., Derode, A., Prada, C., Roux, P., Tanter, M., Thomas, J.L., and Wu, F., 2000, Time-reversed acoustics: Reports on Progress in Physics, v. 63, no. 12, p. 91–113, doi:10.1109/58.710586.

Fink, M., and Prada, C., 2001, Acoustic time-reversal mirrors: Inverse Problems, v. 17, no. 1, p. R1–R38, doi:10.1088/0266-5611/17/1/201.

Goldstein, P., Dodge, D., Firpo, M., and Minner, L., 2003, SAC2000: Signal Processing and Analysis Tools for Seismologists and Engineers Peter Goldstein, Doug Dodge, and Mike Firpo, Lee Minner Lawrence Livermore National Laboratory: Invited contribution to "The IASPEI International Handbook of Earthquake and Engineering Seismology, , no. Academic Press, London, p. 1–7.

Helffrich, G., Wookey, J., and Bastow, I., 2013, The Seismic Analysis Code: A Primer and User's Guide: Cambridge University Press.

Hennino, R., Trégourès, N., Shapiro, N.M., Margerin, L., Campillo, M., Tiggelen, B.A.V., Weaver, R.L., van Tiggelen, B.A., and Weaver, R.L., 2001, Observation of equipartition of seismic waves: Physical Review Letters, v. 86, no. 15, p. 3447–3450, doi:10.1103/PhysRevLett.86.3447.

Klein, F.W., 2014, User's Guide to HYPOINVERSE-2000, a Fortran Program to Solve for Earthquake Locations and Magnitude: U. S. Geological Survey, Open File Report 02-171.

Kwiatek, G., MartínezGarzón, P., and Bohnhoff, M., 2016, HybridMT: A MATLAB/Shell Environment Package for Seismic Moment Tensor Inversion and Refinement: Seismological Research Letters, v. 87, no. 4, p. 964–976, doi:10.1785/0220150251.

Lecocq, T., Caudron, C., and Brenguier, F., 2014, MSNoise, a Python Package for Monitoring Seismic Velocity Changes Using Ambient Seismic Noise: Seismological Research Letters, v. 85, no. 3, p.

715–726, doi:10.1785/0220130073.

Liu, Y., Draganov, D., Wapenaar, K., and Arntsen, B., 2015, Creating Virtual Receivers from Drill-bit Noise, *in* 77th eage conference & exhibition 2015: June, p. 1–4, doi:10.3997/2214-4609.201413571.

Liu, Y., Draganov, D., Wapenaar, K., and Arntsen, B., 2016, Retrieving virtual reflection responses at drill-bit positions using seismic interferometry with drill-bit noise: Geophysical Prospecting, v. 64, no. 2, p. 348–360, doi:10.1111/1365-2478.12292.

Lobkis, O.I., and Weaver, R.L., 2001, On the emergence of the Green's function in the correlations of a diffuse field: The Journal of the Acoustical Society of America, v. 110, no. 6, p. 3011–3017, doi:10.1121/1.1417528.

Lund Snee, J.E., and Zoback, M.D., 2016, State of stress in Texas: Implications for induced seismicity: Geophysical Research Letters, v. 43, no. 19, p. 10,208–10,214, doi:10.1002/2016GL070974.

Madariaga, R., 2007, Seismic Source Theory, *in* Treatise on geophysics: 1963, Elsevier, p. 59–82, doi:10.1016/B978-044452748-6.00061-4.

Matzel, E., Morency, C., Myers, S., Templeton, D., Pyle, M., and Ave, E., 2015, Virtual Seismometers in Geothermal Systems : Using Microquakes to Illuminate the Subsurface: Fourtieth Workshop on Geothermal Reservoir Engineering, , no. figure 1, p. 1–4.

Matzel, E., Morency, C., Rhode, A., Templeton, D., and Pyle, M., 2016, Virtual Seismometers in Geothermal Systems: Looking Inside the Microseismic Cloud: PROCEEDINGS Geothermal Reservoir Engineering Stanford University.

Matzel, E., White, J., Templeton, D., Pyle, M., Morency, C., and Trainor-Guitton, W., 2014, Microseismic techniques for avoiding induced seismicity during fluid injection: Energy Procedia, v. 63, p. 4297–4304, doi:10.1016/j.egypro.2014.11.465.

Melo, G., and Malcolm, A., 2011, SVD enhanced seismic interferometry for traveltime estimates between microquakes, *in* Seg technical program expanded abstracts 2011: Society of Exploration Geophysicists, p. 1608–1612, doi:10.1190/1.3627510.

Melo, G., Malcolm, A., and Fehler, M., 2012, Comparison of microearthquake locations using seismic interferometry principles, *in* Seg technical program expanded abstracts 2012: Society of Exploration Geophysicists, p. 1–5, doi:10.1190/segam2012-1371.1.

Morency, C., and Matzel, E., 2017, SGP-TR-212: Virtual Seismometers for induced seismicity monitoring and full moment tensor inversion, *in* Proceedings, 42nd workshop on geothermal reservoir engineering: p. 1–5.

Newman, R., Clark, A., Trabant, C., Karstens, R., Hutko, A., Casey, R., and Ahern, T., 2013, Wilber 3: A Python-Django Web Application For Acquiring Large-scale Event-oriented Seismic Data: AGU Fall Meeting Abstracts.

Omori, F., 1905, Horizontal pendulum observations of earthquakes in Tokyo: Similarity of the seismic motion originating at neighbouring centres: Publications of the Earthquake Investigation Committee, v. 21, p. 9–102.

Owens, T.J., Crotwell, H.P., Groves, C., and Oliver-Paul, P., 2004, SOD: Standing Order for Data: Seismological Research Letters, v. 75, no. 4, p. 515–520, doi:10.1785/gssrl.75.4.515-a.

Poliannikov, O.V., 2011, Retrieving reflections by source-receiver wavefield interferometry: Geophysics, v. 76, no. 1, p. SA1, doi:10.1190/1.3524241.

Poliannikov, O.V., Rondenay, S., and Chen, L., 2012, Interferometric imaging of the underside of a subducting crust: Geophysical Journal International, v. 189, no. 1, p. 681–690, doi:10.1111/j.1365-246X.2012.05389.x.

Prieto, G.A., Denolle, M., Lawrence, J.F., and Beroza, G.C., 2011, On amplitude information carried by the ambient seismic field: Comptes Rendus - Geoscience, v. 343, no. 8-9, p. 600–614, doi:10.1016/j.crte.2011.03.006.

Rayleigh, J.W.S., 1896, The theory of sound, v. 2: Macmillan, 340 p., doi:10.1038/058121a0.

Rickett, J., and Claerbout, J., 1999, Acoustic daylight imaging via spectral factorization: Helioseismology and reservoir monitoring: The Leading Edge, v. 18, no. 8, p. 957–960, doi:10.1190/1.1438420.

Roux, P., and Fink, M., 2003, Green's function estimation using secondary sources in a shallow water environment.: The Journal of the Acoustical Society of America, v. 113, no. 3, p. 1406–1416, doi:10.1121/1.1542645.

Sabra, K.G., Gerstoft, P., Roux, P., Kuperman, W.A., and Fehler, M.C., 2005, Extracting time-domain Green's function estimates from ambient seismic noise: Geophysical Research Letters, v. 32, no. 3, p. 1–5, doi:10.1029/2004GL021862.

Sato, H., 1977, Energy Propagation Including Scattering Effects, Single Isotropic Scattering Approximation: J. Phys. Earth, v. 25, p. 27–41, doi:10.4294/jpe1952.25.27.

Sato, H., and Fehler, M.C., 2012, Seismic Wave Propagation and Scattering in the Heterogeneous Earth:Second Edition: 1–11 p.

Schoenball, M., and Ellsworth, W.L., 2017, Waveform relocated earthquake catalog for Oklahoma and Southern Kansas illuminates the regional fault network: Seismological Research Letters, doi:10.1785/0220170083.

Schuster, G.T., 2001, A-032: Theory of daylight/interferometric imaging: Tutorial, *in* Eage 63rd conference & technical exhibition: June, p. 4.

Shapiro, N.M., Campillo, M., Stehly, L., and Ritzwoller, M.H., 2005, High-Resolution Surface-Wave Tomography from Ambient Seismic Noise: Science, v. 307, no. 5715, p. 1615–1618, doi:10.1126/science.1108339.

Shearer, P.M., 2009, Introduction to Seismology: Cambridge, Cambridge University Press, doi:10.1017/CBO9780511841552.

Snieder, R., 2004, Extracting the Green's function from the correlation of coda waves: a derivation based on stationary phase.: Physical review. E, Statistical, nonlinear, and soft matter physics, v. 69, no. 4 Pt 2, p. 046,610, doi:10.1103/PhysRevE.69.046610.

Snieder, R., Fan, Y., Slob, E., and Wapenaar, K., 2010, Equipartitioning is not sufficient for Green's function extraction: Earthquake Science, v. 23, no. 5, p. 403–415.

Spudich, P., and Bostwick, T., 1987, Studies of the Seismic Coda Using an Earthquake Cluster as a Deeply Buried Seismograph Array: Journal of Geophysical Research, v. 92, no. B10, p. 526–546, doi:10.1029/JB092iB10p10526.

van Manen, D.J., Curtis, A., and Robertsson, J.O., 2006, Interferometric modeling of wave propagation in inhomogeneous elastic media

using time reversal and reciprocity: Geophysics, v. 71, no. 4, p. SI47–SI60, doi:10.1190/1.2213218.

van Manen, D.J., Robertsson, J.O.A., and Curtis, A., 2005, Modeling of wave propagation in inhomogeneous media: Physical Review Letters, v. 94, no. 16, p. 164,301, doi:10.1103/PhysRevLett.94.164301.

van Manen, D.J., Robertsson, J.O.A., and Curtis, A., 2007, Exact wave field simulation for finite-volume scattering problems: The Journal of the Acoustical Society of America, v. 122, no. 4, p. EL115–EL121, doi:10.1121/1.2771371.

Waldhauser, F., and Ellsworth, W.L., 2000, A Double-difference Earthquake location algorithm: Method and application to the Northern Hayward Fault, California: Bulletin of the Seismological Society of America, v. 90, no. 6, p. 1353–1368, doi:10.1785/0120000006.

Walsh, F.R.I., and Zoback, M.D., 2016, Probabilistic assessment of potential fault slip related to injection-induced earthquakes: Application to north-central Oklahoma, USA: Geology, v. 44, no. 12, p. 991–994, doi:10.1130/G38275.1.

Wapenaar, K., 2004, Retrieving the elastodynamic Green's function of an arbitrary inhomogeneous medium by cross correlation: Physical Review Letters, v. 93, no. 25, p. 1–4, doi:10.1103/PhysRevLett.93.254301.

Wapenaar, K., Draganov, D., Snieder, R., Campman, X., and Verdel, A., 2010, Tutorial on seismic interferometry: Part 1 Basic principles and applications: Geophysics, v. 75, no. 5, p. 75A195–75A209, doi:10.1190/1.3457445.

Wapenaar, K., and Fokkema, J., 2006, Green's function representations for seismic interferometry: Geophysics, v. 71, no. 4, p. SI33, doi:10.1190/1.2213955.

Weaver, R.L., and Lobkis, O.I., 2001, Ultrasonics without a Source : Thermal Fluctuation Correlations at MHz Frequencies: Physical Review Letters, v. 87, no. 13, p. 1–4, doi:10.1103/PhysRevLett.87.134301.

Yang, Y., Ritzwoller, M.H., Levshin, A.L., and Shapiro, N.M., 2007, Ambient noise Rayleigh wave tomography across Europe: Geophysical Journal International, v. 168, no. 1, p. 259–274, doi:10.1111/j.1365-246X.2006.03203.x.